



## Relationships between mechanically induced hydrodynamics and membrane fouling in a novel rotating membrane bioreactor

Tao Jiang<sup>a</sup>, Hanmin Zhang<sup>a,\*</sup>, Fenglin Yang<sup>a</sup>, Dawen Gao<sup>b</sup>, Hai Du<sup>c</sup>

<sup>a</sup>Key Laboratory of Industrial Ecology and Environmental Engineering, MOE, School of Environmental Science and Technology, Dalian University of Technology, Dalian 116024, China

Tel. +86 411 84706172; Fax: +86 411 84708083; email: zhanghm@dlut.edu.cn

<sup>b</sup>State Key Laboratory of Urban Water Resource and Environment, Harbin Institute of Technology, Harbin 150090, China

<sup>c</sup>State Key Laboratory of Coastal and Offshore Engineering, Dalian University of Technology, Dalian 116024, China

Received 22 May 2012; Accepted 12 September 2012

---

### ABSTRACT

The influence of mechanically induced hydrodynamics on membrane fouling in a novel rotating flat-sheet membrane bioreactor (RFMBR) with the comparison of a common membrane bioreactor (CMBR) is analyzed here by the particle image velocimetry (PIV). Obtained results suggest that the fluid velocity has a slight impact on membrane fouling. With the increase in fluid velocity, the membrane fouling does not necessarily mitigate. In contrast, the variations in turbulence intensity have a great negative correlation with the changes in membrane fouling rate for both MBRs, which means that the turbulence induced by fluctuating velocities is helpful for the alleviation of membrane fouling. When comparing the membrane fouling between RFMBR and CMBR, it can be concluded that the membrane fouling rate for RFMBR is much slower compared to CMBR when consuming the same energy, indicating a more outstanding filtration performance of RFMBR.

*Keywords:* Hydrodynamics; Membrane bioreactor (MBR); Membrane fouling; Particle image velocimetry (PIV)

---

### 1. Introduction

Membrane bioreactors (MBRs) combine conventional activated sludge (CAS) system and advanced membrane separation, having been receiving considerable worldwide popularity and attention because of the outstanding merits compared to CAS processes, such as excellent effluent quality, less sludge production, and smaller footprints [1–4]. Nonetheless, membrane fouling, which reduces the effectiveness of reactor and

efficiency of membrane material, is one of the toughest challenges that hamper wide application of MBRs.

It is proven that enhancement of hydrodynamic conditions is one of the effective ways to mitigate membrane fouling [5,6]. In most previous studies, enhancement of hydrodynamic conditions is achieved by introduction of the gas phase, i.e. the turbulence is generated by aeration. However, turbulence promotion by aeration needs large bubbles [7], leading to a low oxygen transfer efficiency. Intense aeration may also damage flocs structure through releasing extracel-

---

\*Corresponding author.

lular polymeric substances (EPS) as well as reducing flocs size, resulting in the deterioration of membrane fouling [8,9]. In addition, when using MBRs to operate anaerobic processes such as anaerobic ammonium oxidation (ANAMMOX), employing aeration to enhance hydrodynamic conditions is unpractical.

Lately, shear-enhanced membrane filtration with a moving membrane module to mitigate membrane fouling has gained much attention [10–15]. In 2010, Zuo et al. [16] proposed a new bioreactor called submerged rotating membrane bioreactor (SRMBR), the membrane module of which comprised several rotatable round PVDF flat-sheets. The equilibrium permeate flux rose from 42.5 to 47.5 L/(m<sup>2</sup>h) as the rotary speed of membrane plates increased from 15 to 25 r/min, proving that rotation of membrane module could enhance shear forces on membrane surface and mitigate membrane fouling. Nevertheless, it is a pity that details in relationships between hydrodynamics and membrane fouling were not clearly pointed out in previous studies.

In order to better understand the effect of mechanically induced hydrodynamics on membrane fouling, a new rotating flat-sheet membrane bioreactor (RFMBR) was made and investigated in this study. Compared to SRMBR, the turbulence and shear forces created by the membrane module of RFMBR are more intense because of its unique rotatable multi-flat-sheet structure (Section 2.1.1). The particle image velocimetry (PIV) system was employed to investigate the hydrodynamics in the new reactor. The PIV is a technique that can provide instantaneous velocity field and related properties in fluids [17], and has been successfully applied to many areas of fluid mechanics [18–21]. Moreover, the relationships between hydrodynamics and membrane fouling in a conventional membrane bioreactor (CMBR) were also discussed in order to provide a comparison with RFMBR.

## 2. Materials and methods

### 2.1. Experimental set-up

#### 2.1.1. Rotating flat-sheet membrane bioreactor

A schematic diagram of the RFMBR is shown in Fig. 1(A). The membrane module is composed of nine identical flat-sheets and two isometric plates that are placed top and bottom, which is installed in a cylindrical reactor with an internal diameter of 240 mm and a total effective volume of 13 L. The reactor and membrane module are made of acrylic glass. The diameter of each plate is 160 mm and the effective height and width of each flat-sheet is 153 and 39 mm, respectively. The two sides of the flat-sheet are covered with polypropylene nonwoven fabric (NWF) with an average pore size of 3 μm (Tianjin TEDA Clean Material Co., Ltd., China).

Several baffles are constructed on the inner wall of the flat-sheets in order to prevent NWF being depressed excessively under pressure. The total effective filtration area is 0.09 m<sup>2</sup>. The flat-sheets are placed vertically on the edge of the plates symmetrically and can be taken out conveniently from the plates when replacing NWF is necessary. The angle between plane of each flat-sheet and its corresponded radius is alterable and is fixed at 30° in this study (Fig. 1(B)). The inside of the lower plate is hollow, and is connected with an external outlet pipe. The hub of the lower plate is connected with gears (gear ratio is 2) that are driven by an adjustable speed electromotor. Hence, driven by the motor, the membrane module could rotate at a designed speed. To control the temperature inside, the reactor is also equipped with three electric heaters at the bottom distributed evenly.

#### 2.1.2. Conventional membrane bioreactor

The material, internal diameter, and total effective volume of CMBR (Fig. 1(C)) are the same as those of RFMBR. Two flat-sheet membrane modules made of acrylic glass with baffles on the inner wall are vertically and symmetrically placed in two sides of the reactor. The membrane material is the same NWF as that used in RFMBR, and the total effective filtration area is also 0.09 m<sup>2</sup>. An outlet connected with external outlet pipe is opened on the bottom of each module. The reactor is equipped with a mechanical stirrer, driven by an electromotor, in the middle in order to mix uniformly. The stirrer is about 5 cm above the bottom of the reactor. The electromotor is placed on the cover of the reactor, and is the same as that in RFMBR.

#### 2.1.3. Energy consumption of the MBRs

The process involved in energy consumption in the microfiltration is the rotation of membrane module and stirrer for RFMBR and CMBR, respectively. The module and stirrer were driven by the electromotor, the real power of which can be determined based on the following expression:

$$P = \frac{Fv}{\eta} \quad (1)$$

where,  $P$  is the real power of electromotor (W),  $F$  is resistance (N),  $v$  is velocity (m/s), and  $\eta$  is the efficiency of electromotor.

The membrane module of RFMBR is driven by a driven gear and a drive gear connected to the electromotor with the gear ratio of 2, while the stirrer of CMBR is directly driven by a same electromotor. Accordingly, at the same rotary speed, the consumed energy of membrane module in RFMBR is twice as

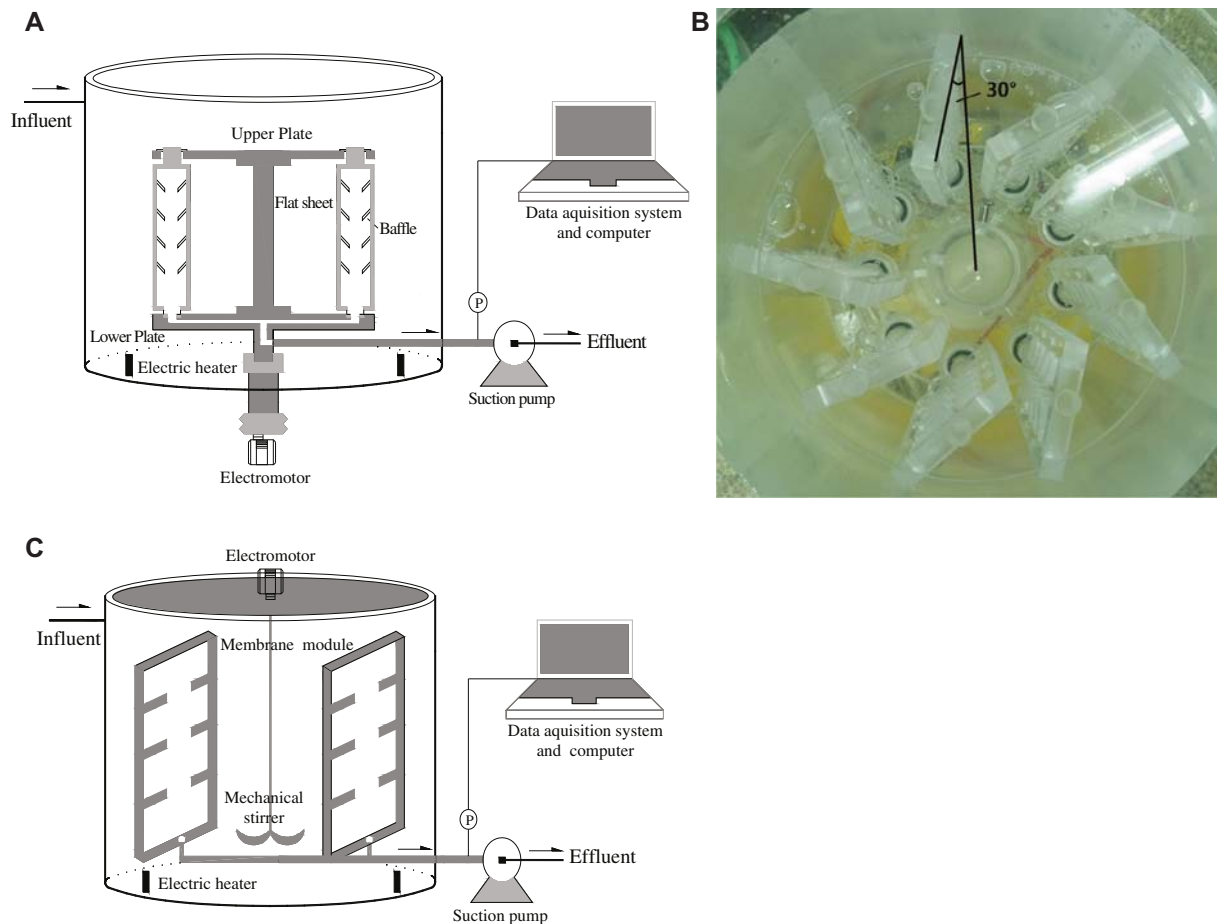


Fig. 1. Schematic diagram of (A) rotating flat-sheet membrane reactor, (B) the arrangement of flat-sheets viewing from the top, and (C) conventional membrane reactor.

much as that of stirrer in CMBR. For example, the energy consumed by CMBR at a stirrer rotary speed of 10 r/min is the same as that by RFMBR at a membrane module rotary speed of 5 r/min. On the basis of above expression, the real power of electromotor is regarded as being proportional to actual rotary speed, while rated power is corresponded to maximal speed. The rated power and maximal speed of the electromotor is 45 W and 90 r/min, respectively. So, the real power of electromotor for RFMBR at the module rotary speed of 5 r/min and CMBR at the stirrer rotary speed of 10 r/m is 5 W, and the energy consumption per  $\text{m}^3$  product water at the flux of  $105 \text{ L}/(\text{m}^2 \text{ h})$  can be calculated to  $0.53 \text{ kWh}/\text{m}^3$  product water. The energy consumption of the MBRs at other speeds can be determined by the ratio of the speed.

## 2.2. The PIV measurement system and instrumentation

The PIV system (TSI, USA) is composed of a charge coupled device (CCD) camera with  $1600 \times 1200$  pixel

resolution, a high power double-pulsed Nd: yttrium aluminium garnet (YAG) laser, a synchronizer, and a signal processing system. The commercial software (TSI INSIGHT 3G) was used to perform image processing. A standard fast Fourier transform (FFT) cross-correlation algorithm was applied and the Gaussian peak detection algorithm was employed to identify the velocity vectors. The interrogation spots had a size of  $32 \times 32$  pixels with a 50% overlap. Pine pollen (mean particle diameter =  $30 \mu\text{m}$ , specific density =  $1.05 \text{ g}/\text{m}^3$ ) were utilized as tracer particles and clean water was adopted as experimental liquid. The particle relaxation time is in the order of  $10^{-8} \text{ s}$ , which is much shorter than the time interval between successive exposures.

In the experiments, the flat-sheets of RFMBR and membrane modules of CMBR were replaced with one-piece glass in order to simulate practical conditions and allow laser to pass through. For RFMBR, the laser light sheet was parallel to the rotary plates and located at the middle of the flat-sheets. The images were acquired by the CCD camera placed

above the reactor. For CMBR, the light sheet was parallel to inside of one membrane module. The CCD camera acquired images from side of the reactor (Fig. 2(A) and (B)). The sizes of images captured by camera in RFMBR and CMBR were  $192.0\text{ mm} \times 143.0\text{ mm}$ , and  $112.0\text{ mm} \times 83.4\text{ mm}$ , respectively. Two images captured in RFMBR and CMBR were shown in Fig. 2(C) and d, respectively. Both of the rotating directions of membrane module and stirrer are anticlockwise viewing from the top.

### 2.3. Microfiltration experiments

Hydrodynamic conditions in the two reactors were changed through altering rotary speed of membrane module and stirrer, respectively. Ten membrane filtration tests were carried out, and each test lasted for 4 h. For the four filtration tests performed with RFMBR, the rotary speed of membrane module was 5, 10, 15, and 25 r/min, respectively; while, for the six

tests with CMBR, the rotary speed of stirrer was 10, 20, 30, 50, 70, and 80 r/min, respectively. The flux was controlled at around  $105\text{ L}/(\text{m}^2\text{ h})$  for each test. The reactor was operated at the temperature of  $25^\circ\text{C}$  by electric heaters. The NWF was renewed after each test to make sure the condition and performance of membrane modules remained the same in all tests. The mixed liquor suspended solids (MLSS) was measured according to standard methods for the examination of water and wastewater described in detail by American Public Health Association (APHA) [22]. The flocs size of suspended solids distribution was determined using a laser granulometer (Mastersizer 2000, Malvern Instruments, UK).

#### 2.3.1. Yeast suspensions

Experiments were conducted with suspensions of active dry baker's yeast (Guangdong Danbaoli Yeast Co., Ltd., China) resuspended in distilled water

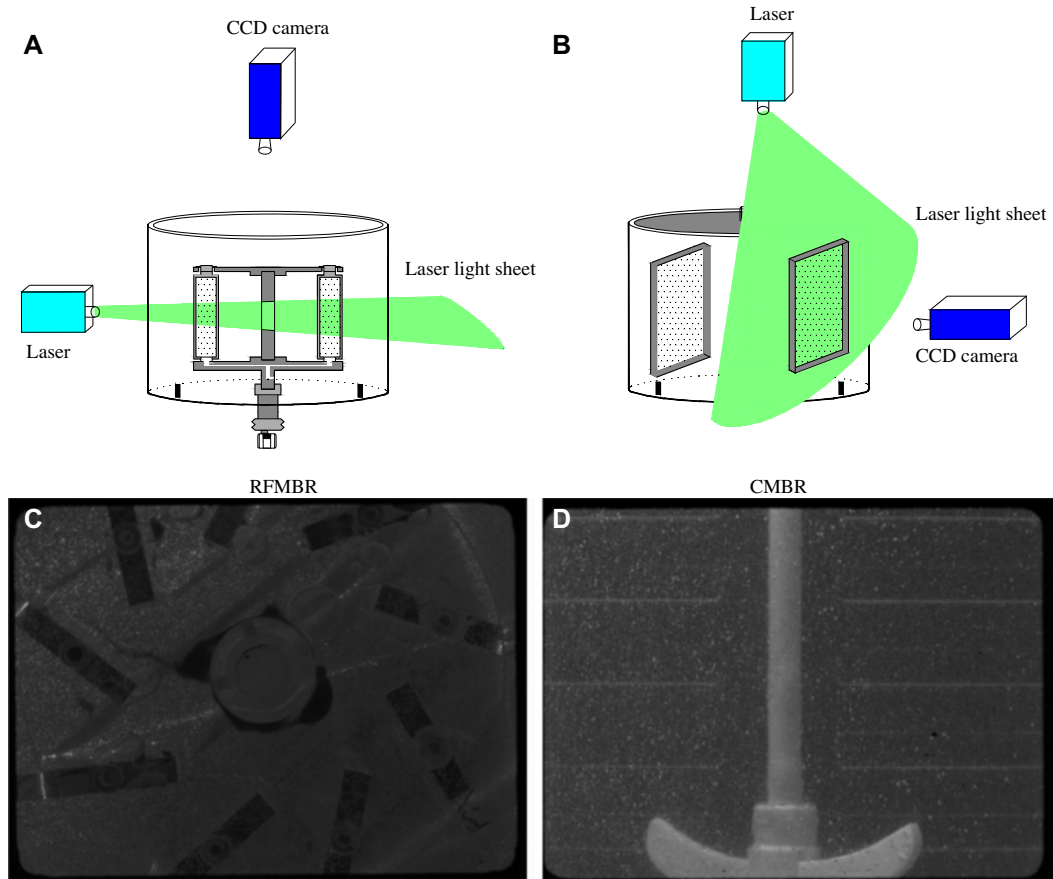


Fig. 2. The position of laser generator and CCD camera in PIV measurement: (A) RFMBR and (B) CMBR; and images captured in (C) RFMBR and (D) CMBR.

and prepared freshly before use. Baker yeast suspensions are commonly used as a “model” biological suspension [6,23]. Indeed, this kind of suspension is used since it contains biomass and colloids with relatively reproducible characteristics. The steps were detailed by Ní Mhurchú and Foley [24]. The mean particle size of used suspensions is  $5.779\ \mu\text{m}$  and the MLSS is  $4.882\ \text{g/L}$ .

### 2.3.2. Characterization of membrane fouling

Membrane fouling is characterized by trans-membrane pressure (TMP), which is measured with pressure sensors (AOB 131, Shanghai Aobo Automation Equipment Co., Ltd., China). The pressure sensors are connected to a 32-channel data acquisition system (PISO-813, ICP-DAS) linked with a personal computer via a PCI interface.

## 3. Results and discussion

### 3.1. Analysis of velocity field

#### 3.1.1. Instantaneous and time-averaged velocity field

Fig. 3 shows an example of comparisons between the instantaneous velocity profiles derived from a single image pair (three images have been selected at random from a string of 50 and shown as Fig. 3(a–c)) and the averaged velocity field (Fig. 3(d)) for CMBR at stirrer rotary speed of  $10\ \text{r/min}$ . The time-averaged flow exhibits a uniform and clear state; in contrast, instantaneous flow shows random and unsteady variation. Most likely, the random vectors in the instantaneous flow field are caused by a correlation between the two consecutive frames that is too weak, and averaging these flow fields over time will eliminate these random and deviations. Also, as will be discussed below, the velocity profiles shown here are average of 50 instantaneous velocity profiles.

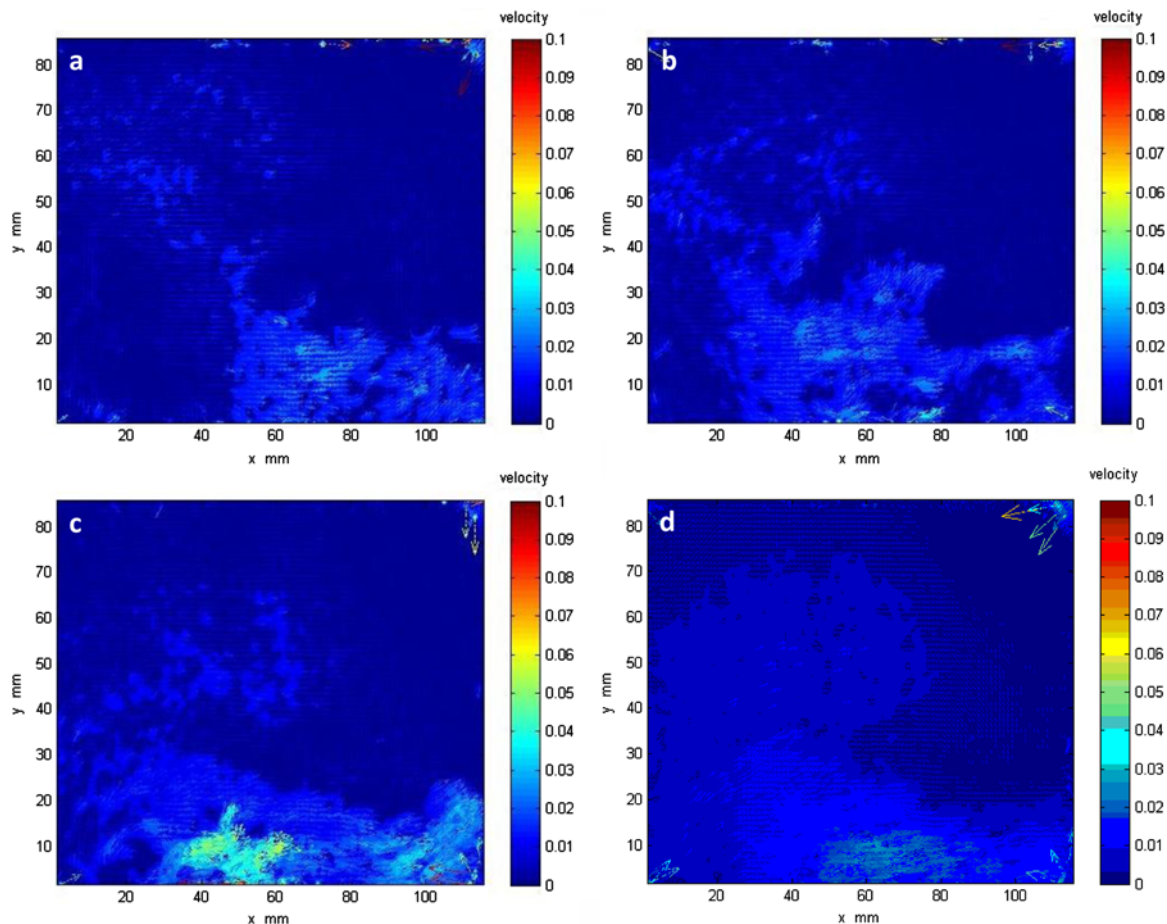


Fig. 3. Instantaneous and time-averaged velocity field in conventional membrane bioreactor (at stirrer rotary speed of  $10\ \text{r/min}$ ). (a), (b), and (c) instantaneous velocity fields and (d) time-averaged velocity field. The unit of velocity legend is  $\text{m/s}$ .

### 3.1.2. Velocity field in rotating plate membrane bioreactor

The flow fields in rotating plate membrane bioreactor were shown in Fig. 4 as membrane module rotated. It can be observed from Fig. 4 that the fluid velocity in reactor increases with the increase in membrane module rotary speed. At membrane module rotary speed of 5 r/min, the maximal fluid velocity is around 0.04 m/s; as membrane module rotary speed raises to 10 r/min, the maximal fluid velocity increases to about 0.08 m/s; and while, membrane module rotary speed increases to 15 and 25 r/min, the maximal fluid velocity reaches to about 0.12 and 0.20 m/s, respectively.

Analyzing experimental data, typical flow patterns can be observed at the four different membrane module rotary speeds. Take 15 r/min for example, the maximal fluid velocity appears near the rotating plates, and with shifting to the inner part, the fluid velocity decreases gradually. The decrease in the fluid

velocity from rotating plates to inner part shows a clear gradient.

### 3.1.3. Velocity field in conventional membrane bioreactor

Fig. 5 shows the changes in velocity field in conventional membrane bioreactor as stirrer rotary speed increases. Similar to RFMBR, as the stirrer rotates faster, the velocity of fluid in CMBR becomes larger. The maximal fluid velocity, appearing near the stirrer, changes from 0.03 to 0.1 m/s approximately. The direction of the flow at the bottom in pictures captured is from left to right because of the anticlockwise rotation of the stirrer viewing from the top. As shown in Fig. 5, when moving to the upper part, the flow changes to two distinct parts due to the lift force induced by the mechanical stirrer. For the left part, the direction of the flow is upper right; while for the right part, the direction is downward. Thus, a weak recirculation flow zone is formed.

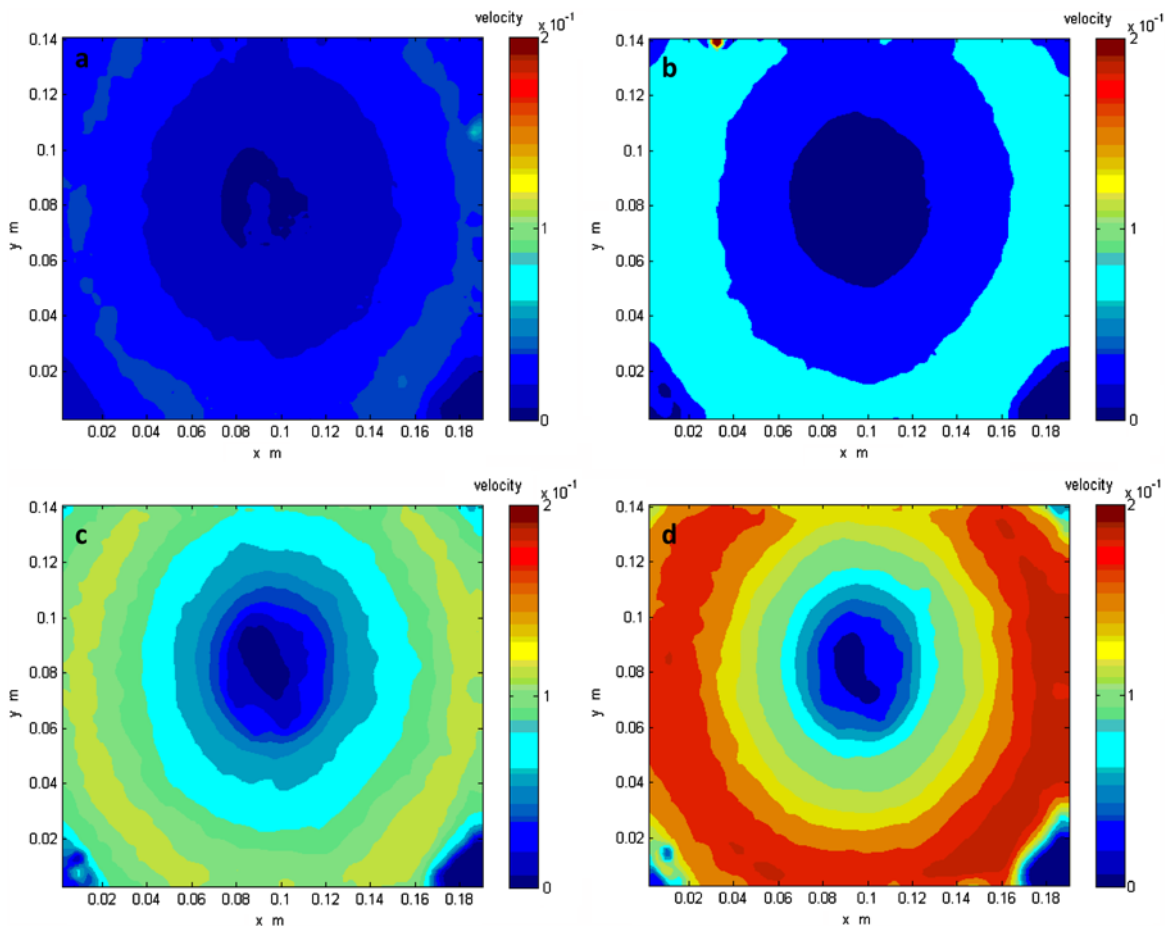


Fig. 4. Time-averaged velocity field in rotating plate membrane bioreactor at membrane module rotary speed of: (a) 5 r/min, (b) 10 r/min, (c) 15 r/min, and (d) 25 r/min. The unit of velocity legend is m/s.

### 3.1.4. Comparison of velocity field between the two bioreactors

Since the energy consumed by membrane module in RFMBR is twice as much as that by stirrer in CMBR

at the same rotary speed, it is reasonable to compare velocity field between the two bioreactors when the rotary speed of stirrer in CMBR is twice as much as that of membrane module in RFMBR. Comparing Fig. 4(a) with Fig. 5(a), one can observe that when

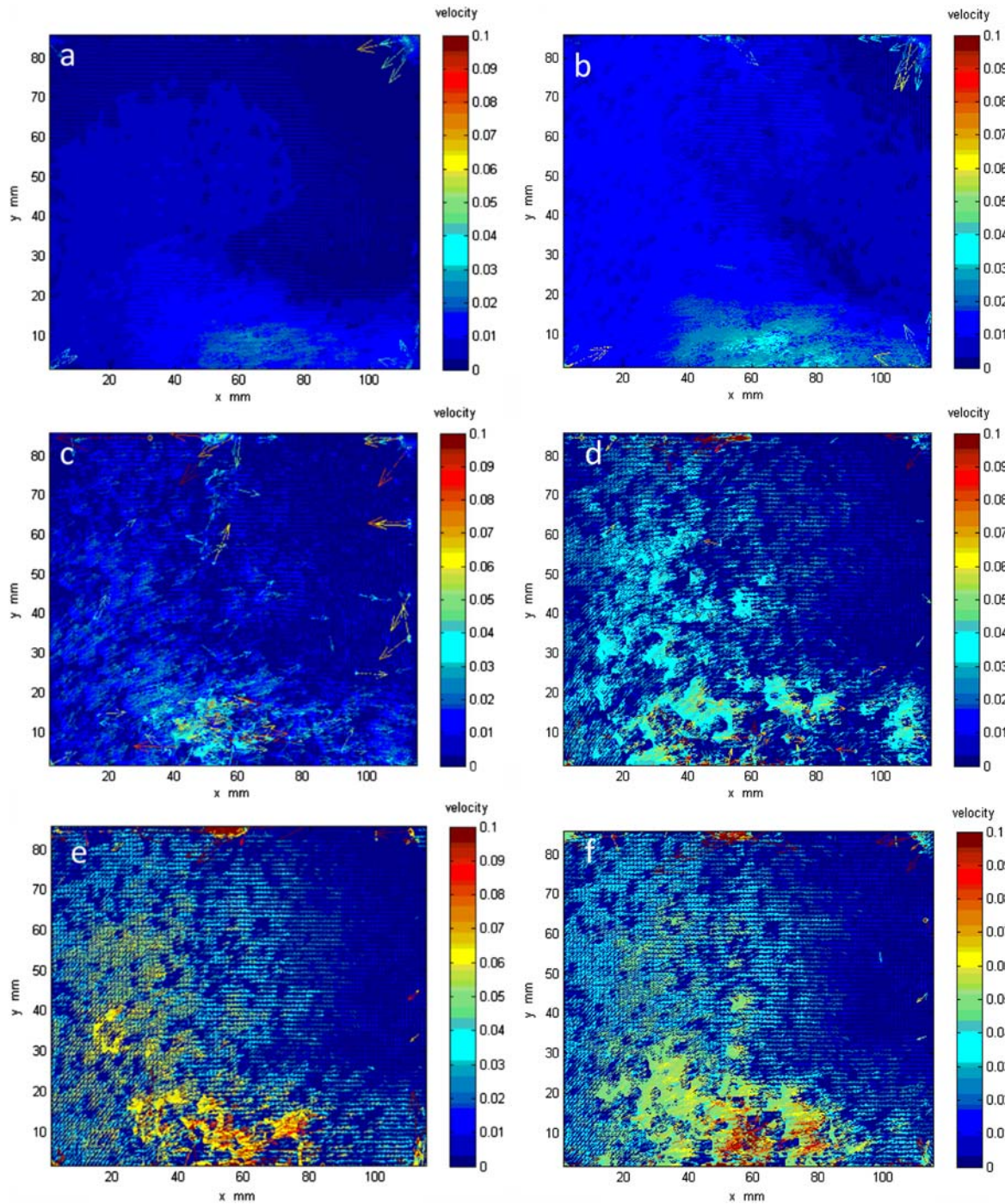


Fig. 5. Time-averaged velocity field in conventional membrane bioreactor at stirrer rotary speed of: (a) 10 r/min, (b) 20 r/min, (c) 30 r/min, (d) 50 r/min, (e) 70 r/min, and (f) 80 r/min. The unit of velocity legend is m/s.

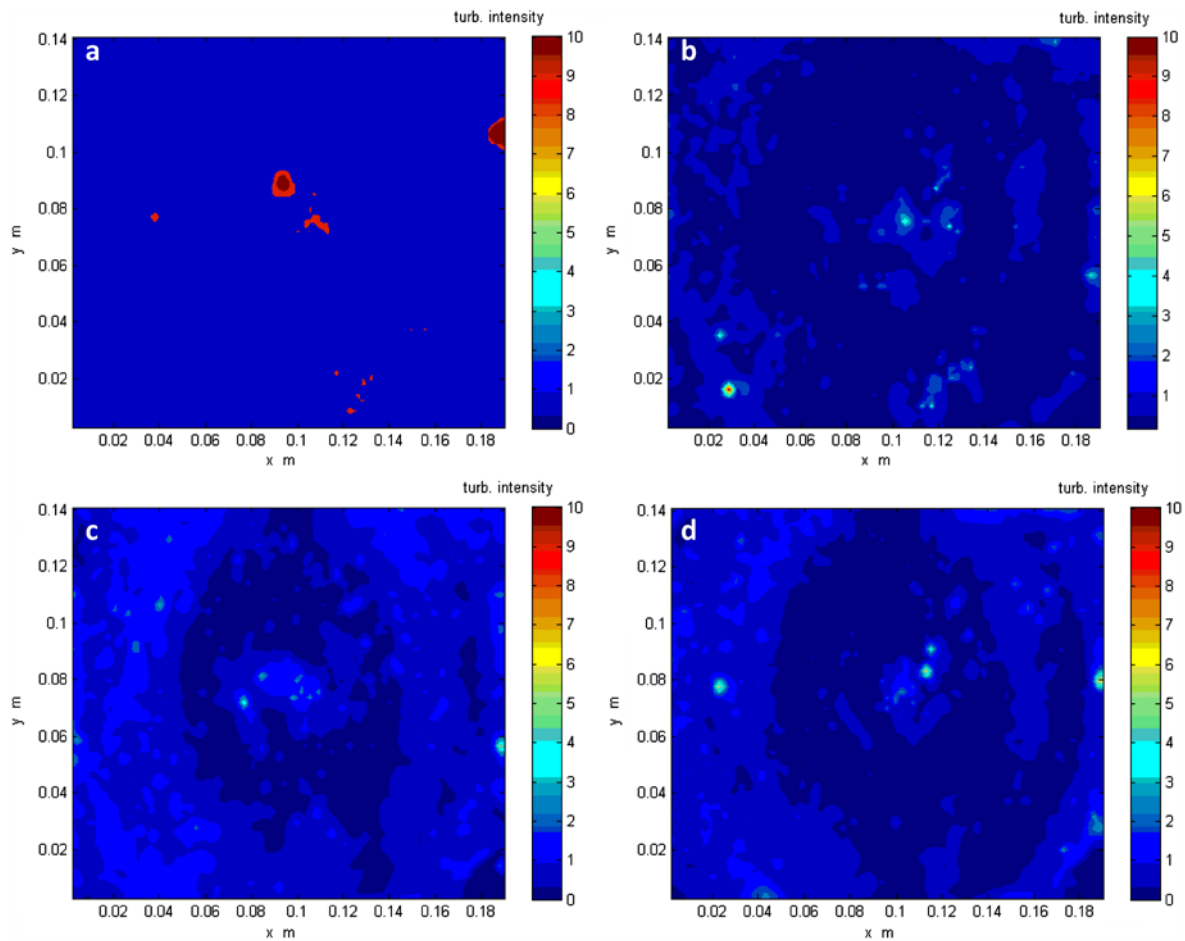


Fig. 6. Turbulence intensity in rotating plate membrane bioreactor at membrane module rotary speed of: (a) 5 r/min, (b) 10 r/min, (c) 15 r/min, and (d) 25 r/min. The turbulence intensity legend is dimensionless.

consuming the same energy, the magnitudes of the fluid velocity in the two bioreactors differ from each other slightly. However, as shown in Figs. 4b and 5b, when rotary speed reaches to 10 and 20 r/min, respectively, the magnitude of the fluid velocity in RFMBR is significantly larger than that in CMBR. While the rotary speed becomes larger, the difference in fluid velocity magnitude between the two reactors becomes more significant. Therefore, it can be concluded that the fluid velocity in RFMBR increases more rapidly than that in CMBR as the rotary speed increases. In other word, the fluid velocity in RFMBR is influenced by rotary speed more significantly than CMBR. Accordingly, the energy used in RFMBR is more efficient than that in CMBR. From Figs. 4 and 5, it can also be seen that the gradient of the velocity is much more obvious for RFMBR than CMBR. So, the shear stress which is related to velocity gradient in RFMBR may be larger than that in CMBR.

### 3.2. Analysis of turbulence intensity

#### 3.2.1. Turbulence intensity in rotating plate membrane bioreactor

In order to investigate the velocity fluctuation and its possible relationship with membrane fouling, turbulence intensity was calculated for the two reactors. Turbulence intensity (TI) is a scale characterizing turbulence expressed as a ratio. The TI is defined in the following equation [25]:

$$\text{T.I.} = \frac{u'}{U} \quad (2)$$

where,  $u'$  is the root-mean-square (RMS), or standard deviation, of the turbulent velocity fluctuations at a particular location over a specified period of time and  $U$  is the average of the velocity at the same location over same time period.

Fig. 6 shows the changes in turbulence intensity in RFMBR as membrane module rotary speed increases. From Fig. 6, it can be observed that, not like fluid velocity, TI does not necessarily increase with the increase in membrane module rotary speed. The maximal average TI appears at rotary speed of 15 r/min,

and at rotary speed of 5 r/min, the TI is approximately 0, indicating that the velocity fluctuation is very weak at 5 r/min. The average TI at rotary speed of 15 r/min is slightly larger than that at rotary speed of 25 r/min, which means a bit more intense turbulence at 15 r/min when compared to turbulence at

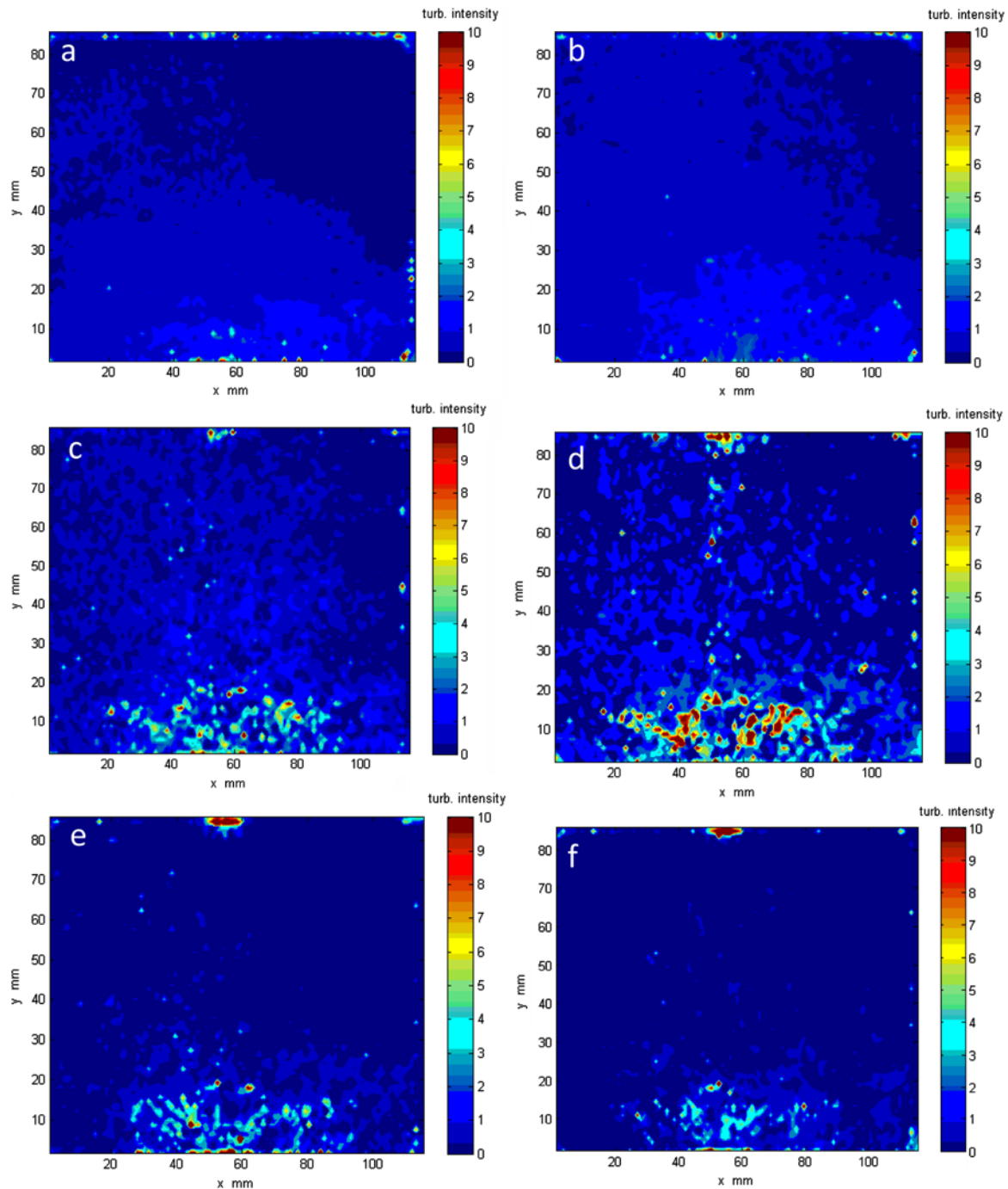


Fig. 7. Turbulence intensity in conventional membrane bioreactor at stirrer rotary speed of: (a) 10 r/min, (b) 20 r/min, (c) 30 r/min, (d) 50 r/min, (e) 70 r/min, and (f) 80 r/min. The turbulence intensity legend is dimensionless.

25 r/min. From Fig. 6, we can also see that for a specific rotary speed, the maximal TI appears near the rotating plates, i.e. the membrane surface, indicating near the membrane surface, the turbulence is most intense for a specific rotary speed.

### 3.2.2. Turbulence intensity in conventional membrane bioreactor

The turbulence intensity in CMBR is shown in Fig. 7. The changing trends in TI in CMBR as stirrer rotary speed increases is similar to that in RFMBR. The maximal average TI appears at rotary speed of 50 r/min, indicating the most intense velocity fluctuation at 50 r/min. As shown in Fig. 7, as stirrer rotary speed raises from 10 to 50 r/min, the average TI increases gradually. However, when stirrer rotary speed ascends from 50 to 70 and to 80 r/min, the average TI decreases. Moreover, like the RFMBR, the maximal TI appears near the stirrer for a specific rotary speed.

### 3.3. Analysis of vortex

The vortex is the motion of the fluid swirling rapidly around a center [26]. Fig. 8 shows vortex variations in the RFMBR, from which we can see that the vorticity increases with the increase in membrane module rotary speed. At the membrane module rotary speed of 5 r/min, the vortex is relatively unapparent, and as the rotary speed is elevated, vortex becomes complete and obvious. Furthermore, it can be seen that vortex shedding, which indicates an unsteady flow, takes place in the reactor. The vortex in the CMBR is very weak (data not shown), which may be due to the very weak recirculation flow formed near the membrane surface.

### 3.4. Membrane fouling rate

The membrane fouling is characterized by TMP collected by pressure sensors every 30 s in the filtration experiments. Due to the tremendous volume of the raw data, which makes the presentation unclear,

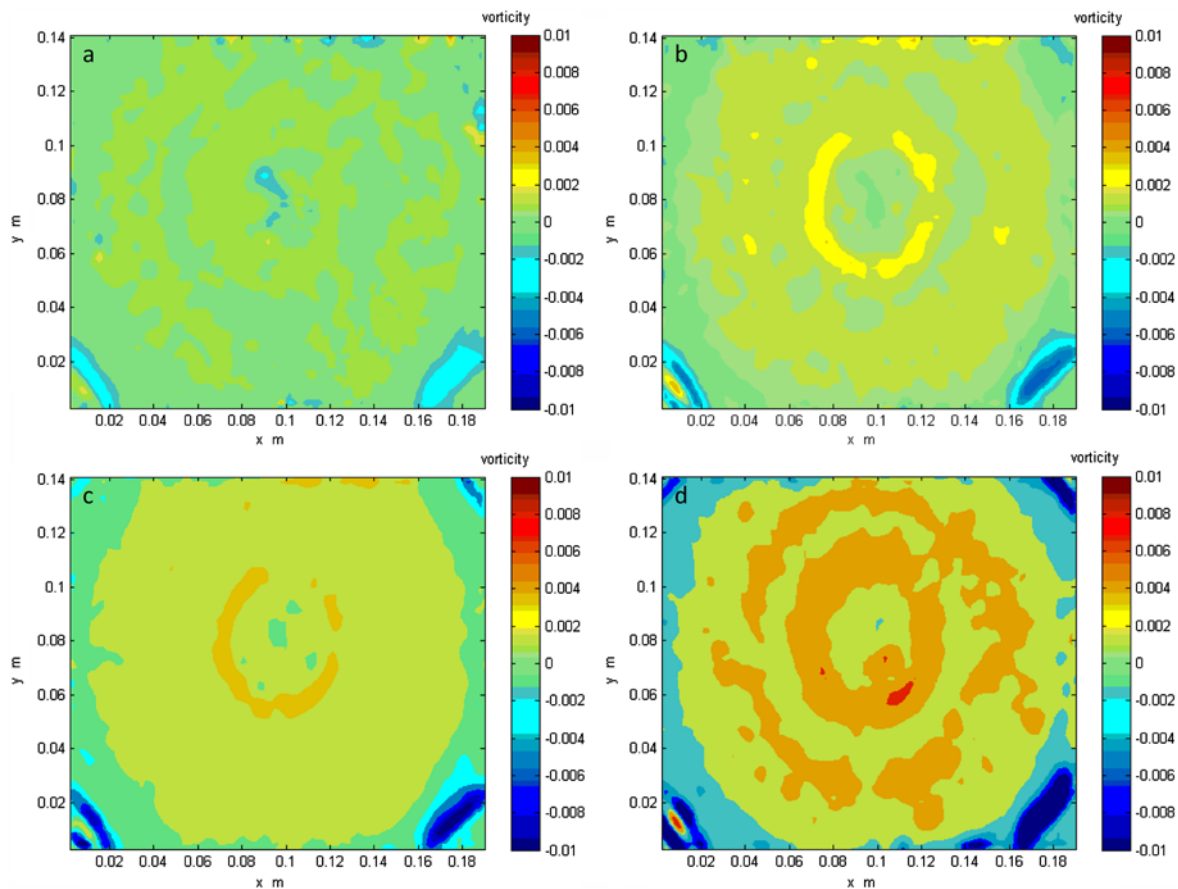


Fig. 8. Changes in vortex in the RFMBR. Membrane module rotary speed of: (a) 5 r/min, (b) 10 r/min, (c) 15 r/min, and (d) 25 r/min. The unit of vorticity legend is  $s^{-1}$ .

the data were treated with the 10-period simple moving average (SMA) method. Fig. 9 shows TMP evolutions in the 4h membrane filtration tests for RFMBR and CMBR. Due to the high flux ( $105 \text{ L}/(\text{m}^2 \text{ h})$ ) and high hydrophobicity of polypropylene NWF, the TMP ascends from 0 to around 25 kPa rapidly within initial 20 min for the 10 filtration tests, and then goes up relatively gently [27]. From Fig. 9, we can see that the rate of TMP rise varies with different rotary speeds, indicating that mechanically induced hydrodynamics indeed has an impact on membrane fouling. However, the rate of TMP rise does not correspond to the increase in rotary speed for both RFMBR and CMBR. In other words, the rate of TMP rise does not necessarily decrease as the rotary speed is elevated. For RFMBR, as membrane module rotary speed increases from 5 to 15 r/min, the rate of TMP rise decreases gradually. Nonetheless, when rotary speed continues to go up to 25 r/min, the rate of TMP rise becomes a bit higher. Similarly, for CMBR, the rate of TMP rise

decreases as stirrer rotary speed increases from 10 to 50 r/min, and with the continuous increase in rotary speed, the rate of TMP rise begins to go up. Comparing the TMP rise between RFMBR and CMBR, we can see that when consuming the same energy, the rate of TMP rise for RFMBR is much slower than that for CMBR, indicating a much more effective way to ameliorate membrane fouling for RFMBR.

### 3.5. Relationships between hydrodynamics and membrane fouling rate

Comparing Figs. 4, 5 and 9, it can be concluded that the increase in fluid velocity is not consequentially helpful for the membrane fouling mitigation. This is somewhat in agreement with results of Zuo et al. [16] indicating that there was a critical rotation speed beyond which a further increase in rotation speed could not further enhance the equilibrium flux for SRMBR. As we know, in MBRs, the mitigation of membrane fouling is mainly dependent on the detachment of foulants from membrane surface attributed mainly to shear forces [5]. The increase in fluid velocity can enhance the velocity of foulants in mixed liquor; however, this has two-sided effect on membrane fouling. On the one hand, the enhancement of foulants velocity is helpful for the detachment of foulants from membrane surface and on the other hand, it can also be benefit for the attachment of foulants to the membrane surface, since the foulants move randomly in the mixed liquor.

Interestingly, it can be observed from Figs. 6, 7 and 9 that the variations in turbulence intensity match very well with the changes in TMP rise for the 10 filtration tests, indicating that TI of the fluid may have the most significant influence on membrane fouling. Yeo et al. [28] investigated hydrodynamic factors affecting the performance of a submerged hollow fiber bundle. They found that there was no any clear relationship between the average velocity and the final TMP measured; however, the increasing standard deviation of velocity improved the performance of the hollow fiber bundle in terms of the final suction pressure. Here, the standard deviation of velocity is similar to turbulence intensity. The reason why TI has a significant influence on membrane fouling may be due to that the fluid velocity fluctuation near the membrane surface becomes more intense with the increase in TI, and this strong fluctuation could make the vibration of foulants on the membrane surface more frequent, and thus are helpful for the detachment of foulants from membrane surface, leading to the amelioration of membrane fouling.

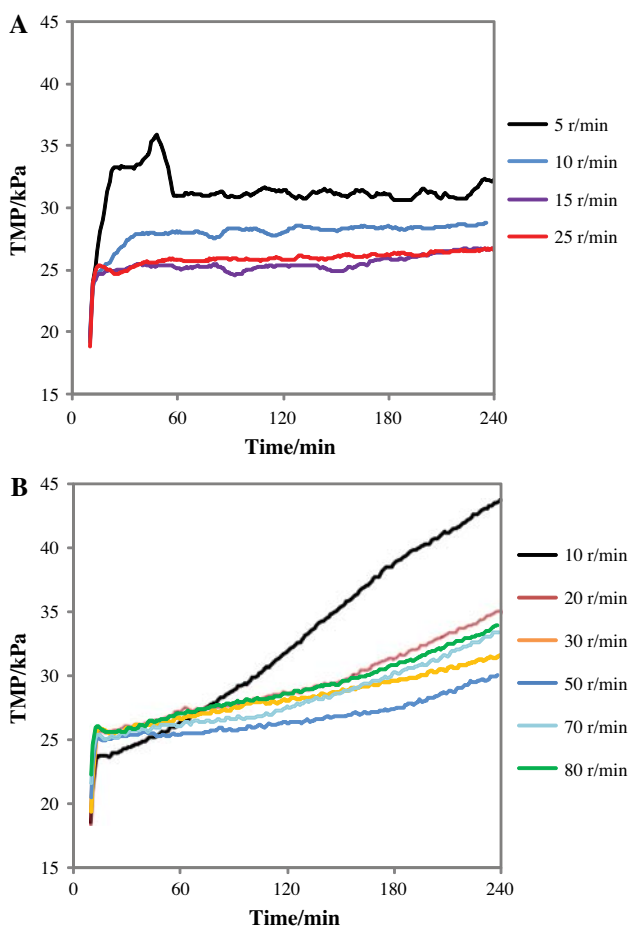


Fig. 9. The TMP rise in the 4h membrane filtration tests for RFMBR and CMBR. (A) RFMBR and (B) CMBR.

#### 4. Conclusions

- The fluid velocity has a slight impact on membrane fouling. With the increase in fluid velocity, the fouling does not necessarily mitigate.
- Membrane fouling is strongly affected by turbulence intensity. In detail, the variations in turbulence intensity have a great negative correlation with the changes in fouling rate, which means the turbulence induced by fluctuating velocities is helpful for alleviating fouling.
- When comparing the membrane fouling between RFMBR and CMBR, it can be concluded that the fouling rate for RFMBR is much slower than that for CMBR when consuming the same energy, indicating a more outstanding filtration performance of RFMBR.

#### Acknowledgments

This work was supported by State Key Laboratory of Urban Water Resource and Environment, Harbin Institute of Technology, China (No. QA200906). The authors would also like to express their sincere appreciation to the Editor and Reviewers for their helpful suggestions and comments.

#### References

- [1] S. Judd, *The MBR Book: Principles and Applications of Membrane Bioreactors for Water and Wastewater Treatment*, Elsevier, Oxford, 2006.
- [2] H.F. Zhang, B.S. Sun, X.H. Zhao, J.M. Sun, Membrane fouling caused by soluble microbial products in an activated sludge system under starvation, *Desalin. Water Treat.* 1 (2009) 180–185.
- [3] Z.W. Wang, Z.C. Wu, G.P. Yu, H.F. Liu, Z. Zhou, Relationship between sludge characteristics and membrane flux determination in submerged membrane bioreactors, *J. Membr. Sci.* 284 (2006) 87–94.
- [4] N. Engelhardt, W. Firk, W. Warnken, Integration of membrane filtration into the activated sludge process in municipal wastewater treatment, *Water Sci. Technol.* 38 (1998) 429–436.
- [5] F.G. Meng, S.R. Chae, A. Drews, M. Kraume, H.S. Shin, F.L. Yang, Recent advances in membrane bioreactors (MBRs): membrane fouling and membrane material, *Water Res.* 43 (2009) 1489–1512.
- [6] Z. Wang, Y. Cui, J. Yao, J. Chu, Y. Liang, The influence of various operating conditions on specific cake resistance in the crossflow microfiltration of yeast suspensions, *Desalin. Water Treat.* 1 (2009) 237–247.
- [7] H. Prieske, A. Drews, M. Kraume, Prediction of the circulation velocity in a membrane bioreactor, *Desalination* 231 (2008) 219–226.
- [8] L. Ji, J.T. Zhou, Influence of aeration on microbial polymers and membrane fouling in submerged membrane bioreactors, *J. Membr. Sci.* 276 (2006) 168–177.
- [9] J.S. Park, K.M. Yeon, C.H. Lee, Hydrodynamics and microbial physiology affecting performance of a new MBR, membrane-coupled high-performance compact reactor, *Desalination* 172 (2005) 181–188.
- [10] M.Y. Jaffrin, Dynamic shear-enhanced membrane filtration: a review of rotating disks, rotating membranes and vibrating systems, *J. Membr. Sci.* 324 (2008) 7–25.
- [11] J. Luo, L.H. Ding, Influence of pH on treatment of dairy wastewater by nanofiltration using shear-enhanced filtration system, *Desalination* 278 (2011) 150–156.
- [12] S. Ahmed, M.G. Rasul, M.A. Hasib, Y. Watanabe, Performance of nanofiltration membrane in a vibrating module (VSEP-NF) for arsenic removal, *Desalination* 252 (2010) 127–134.
- [13] S.C. Low, H.H. Juan, L.K. Siong, A combined VSEP and membrane bioreactor system, *Desalination* 183 (2005) 353–362.
- [14] R. Bouzerar, P. Paullier, M.Y. Jaffrin, Concentration of mineral suspensions and industrial effluents using a rotating disk dynamic filtration module, *Desalination* 158 (2003) 79–85.
- [15] K. Takata, K. Yamamoto, R. Bian, Y. Watanabe, Removal of humic substances with vibratory shear enhanced processing membrane filtration, *Desalination* 117 (1998) 273–282.
- [16] D.Y. Zuo, H.J. Li, H.T. Liu, G.P. Wu, A study on submerged rotating MBR for wastewater treatment and membrane cleaning, *Korean J. Chem. Eng.* 27 (2010) 881–885.
- [17] N.G. Deen, B.H. Hjertager, Particle image velocimetry measurements in an aerated stirred tank, *Chem. Eng. Commun.* 189 (2002) 1208–1221.
- [18] X.A. Mao, A.J. Jaworski, Application of particle image velocimetry measurement techniques to study turbulence characteristics of oscillatory flows around parallel-plate structures in thermoacoustic devices, *Meas. Sci. Technol.* 21 (2010) 1–16.
- [19] M. Raffel, C.E. Willert, S.T. Wereley, J. Kompenhans, *Particle Image Velocimetry: A Practical Guide*, second ed., Springer, Berlin, 2007.
- [20] S.J. Lee, C.W. Park, J.H. Kang, Daichin Evaluation of wind environment around a residential complex using a PIV velocity field measurement technique, *Environ. Fluid Mech.* 9 (2009) 655–668.
- [21] L. Martinelli, C. Guigui, A. Line, Characterisation of hydrodynamics induced by air injection related to membrane fouling behavior, *Desalination* 250 (2010) 587–591.
- [22] APHA (American Public Health Association), *Standard Methods for the Examination of Water and Wastewater*, 19th ed., New York, USA, 1995.
- [23] O. Al-akoum, M. Mercier-Bonin, L. Ding, C. Fonade, P. Aptel, M. Jaffrin, Comparison of three different systems used for flux enhancement: application to crossflow filtration of yeast suspensions, *Desalination* 147 (2002) 31–36.
- [24] J. Ní Mhurchú, G. Foley, Dead-end filtration of yeast suspensions: correlating specific resistance and flux data using artificial neural networks, *J. Membr. Sci.* 281(1–2) (2006) 325–333.
- [25] G.L. Geernaert, S.E. Larsen, F. Hansen, Measurements of the wind stress, heat flux, and turbulence intensity during storm conditions over the North Sea, *J. Geophys. Res.* 92(12) (1987) 13127–13139.
- [26] R.K. Kundu, I.M. Cohen, *Fluid Mechanics*, second ed., Academic Press, San Diego, CA, 2002.
- [27] A. Brookes, B. Jefferson, S.J. Judd, Sub-critical fouling in a membrane bioreactor: impact of flux and MLSS, in: *Proc. IWA 4th World Water Congress*, Marrakech, 2004.
- [28] P.S.A. Yeo, W.K.A. Law, A.G. Fane, Factors affecting the performance of a submerged hollow fiber bundle, *J. Membr. Sci.* 280 (2006) 969–982.